Supplementary Information for

Enhancing the Reliability of Dyes for Color Filters through TiO_2 Adsorption: Comprehensive Identification of Factors Affecting Photocatalysis

Wan Soo Kim [a], So Jeong Park [a], Tae Gyu Hwang [b], Hong Mo Kim [c], Hyun Kyu Lee [a], Suhyeon Kim [a], Woo Jin Choi [a], Jun Ho Yoon [a], Yoo Sang Kim [a], Dong Jun Lee [a], Seong Hyun Jang [d], Jin Young Kim [a, *], and Jae Pil Kim [a, *]

[a] Department of Materials Science and Engineering, Seoul National University, 151-744, Republic of Korea

b Center for Specialty Chemicals, Korea Research Institute of Chemical Technology (KRICT), Ulsan 44412, Republic of Korea

[c] Advanced Institute of Convergence Technology, Suwon 864-1, Republic of Korea

d Material & Component Convergence R&D Department, Korea Institute of Industrial Technology (KITECH), 15588, Republic of Korea

Corresponding author.

E-mails: jaepil@snu.ac.kr

S1. Synthesis and characterization.

S1.1. Synthesis of PBI 2

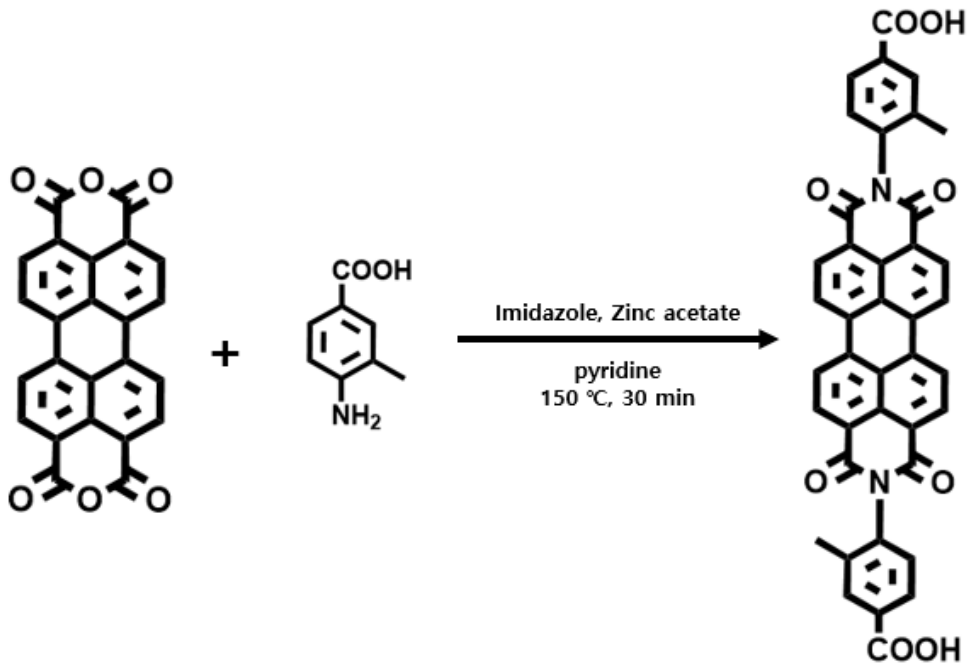

Scheme S1. Synthesis of PBI 2.

3,4,9,10-perylene tetracarboxylic dianhydride (0.3 g, 0.76 mmol), imidazole (2.0 g, 30.0 mmol), zinc acetate (0.024 g, 0.13 mmol) and pyridine (3 mL) were mixed and stirred for 30 min at 150 ℃. Then 4-amino-3-methylbenzoicacid (0.37 g, 2.44 mmol) was added and stirred for 22 h under a nitrogen atmosphere. After the reaction was completed, the mixture was cooled to room temperature, followed by acidizing and filtrating with HCl and water. The precipitate was washed with ethanol

and dried in vacuum to yield pure PBI 2.

Yield: 88%; ^{1}H NMR (500 MHz, N,N-Dimethylformamide-*d7*): δ= 10.42 (s, 2H), 9.18-9.19 (d, J=8.1 Hz, 4H), 7.38 (s, 2H), 7.33-7.34 (d, J= 9.1 Hz, 2H), 7.16-7.17 (d, J= 8.9 Hz, 4H), 6.65-6.66 (d, J= 9.9 Hz, 2H), 2.23 (s, 6H). MALDI-TOF MS: $C_{40}H_{22}N_2O_8$ calculated for: 659.62; found: 660.2186 (100%, [M + H]). Elemental analysis: Calc. for $C_{40}H_{22}N_2O_8$ (%): C, 72.95; H, 3.37; N, 4.25; O, 19.43. Found (%): C, 72.9471; H, 3.3687; N, 4.2534; O, 19.4117.

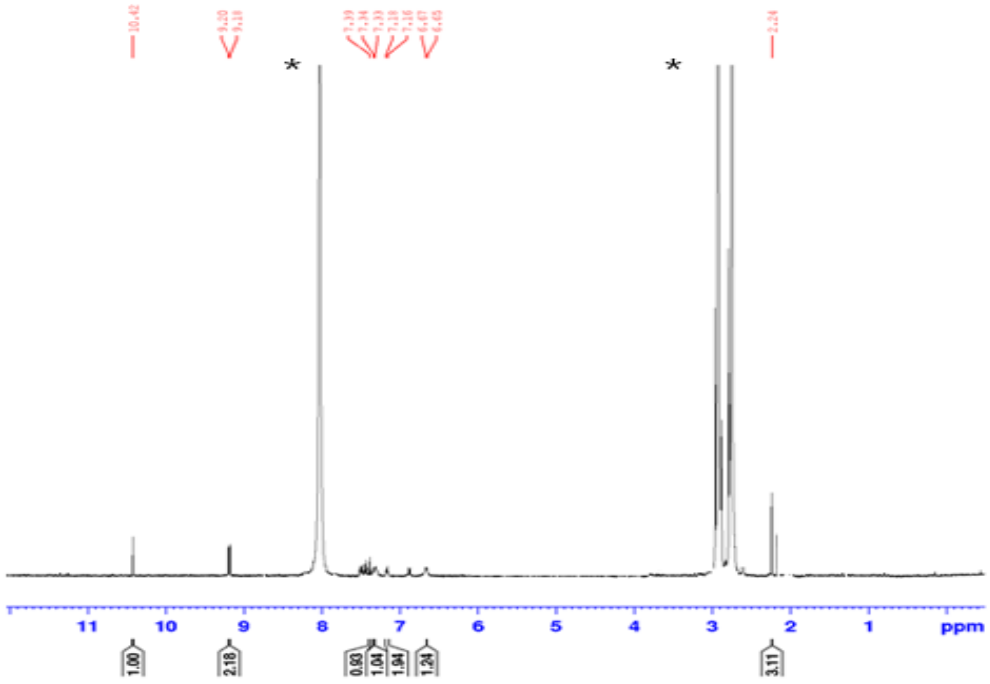

Fig. S1. ^{1}H NMR spectra of PBI 2.

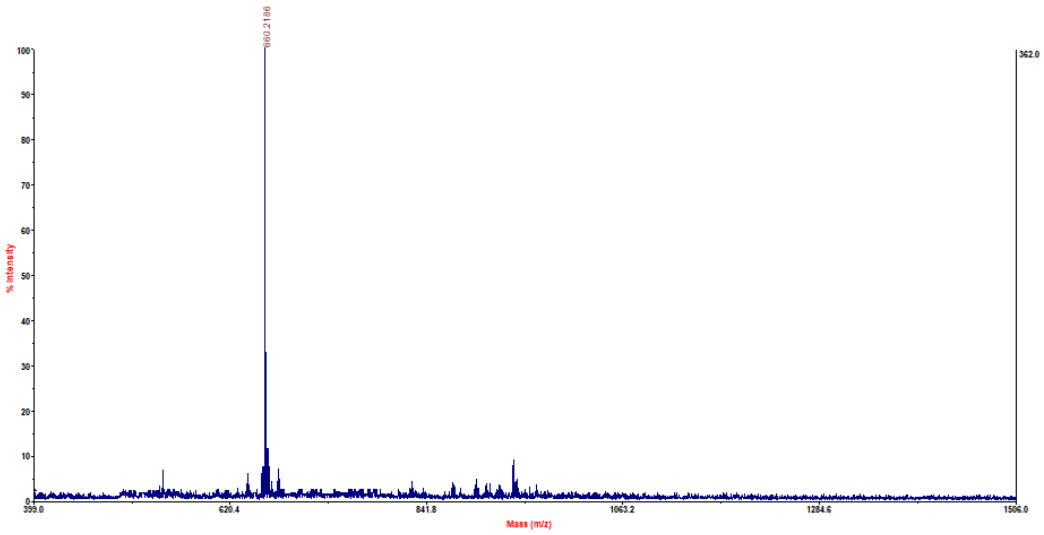

Fig. S2. MALDI-TOF mass spectra of PBI 2.

S1.2.1. DPP-I

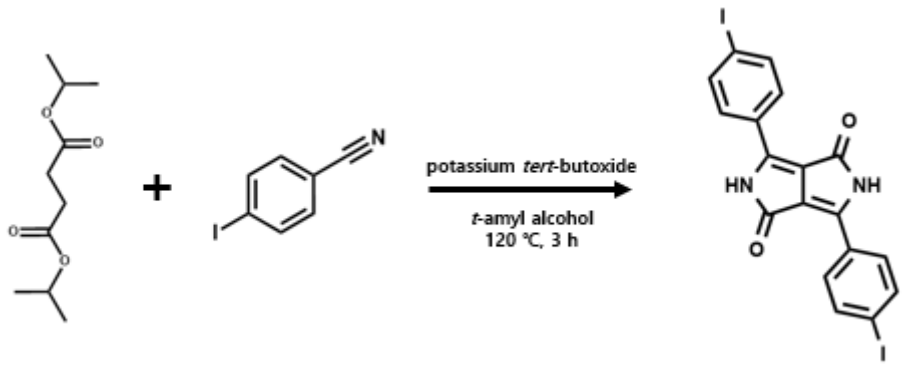

Scheme S2. Synthesis of DPP I.

Potassium *tert*-butoxide (2.58 g, 17.8 mmol), 4-iodobenzonitrile (4.586 g, 20.0 mmol), and *t*-amyl alcohol (17 ml) were mixed and stirred for 30 min at 120 ℃. The mixture of diisopropyl succinate (1.17 g, 8 mmol) and *t*-amyl alcohol (5 ml) was added dropwise, and the resulting mixture was

maintained at this temperature for 3 h under a nitrogen atmosphere. After the reaction was completed, the mixture was cooled to room temperature. The reaction mixture was poured into the acidic MeOH (200 ml of MeOH and 10 ml of concentrated HCl). The precipitate was washed with hot MeOH and water, then filtered and dried in vacuum to yield DPP-I, which was used directly in the subsequent reaction without further purification.

S1.2.2. DPP-I 2

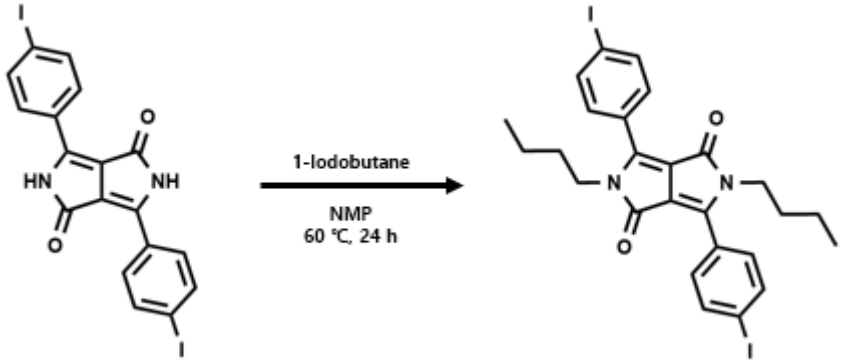

Scheme S3. Synthesis of DPP-I 2.

DPP I (0.2 g, 0.37 mmol), potassium *tert*-butoxide (0.1 g, 8.9 mmol), and NMP (20 ml) were mixed and stirred for 30 min at 60 ℃. Then, 1-iodobutane (0.28 g,1.52 mmol) was added and stirred for

24 h under a nitrogen atmosphere. After the reaction was completed, the mixture was cooled to room temperature. The reaction mixture was then poured into water and extracted with MC. The combined organic layers were dried over anhydrous $MgSO_4$ and dried in vacuum. The crude product was purified by column chromatography using MC solution.

Yield: 47%; ^{1}H NMR (850 MHz, Toluene-*d8*): δ= 7.43-7.44 (d, J=8.73 Hz, 4H), 7.36-7.37 (d, J=8.73 Hz, 4H), 3.51-3.53 (t, J= 7.60 Hz, 4H), 1.38-1.42 (quintet, J= 7.54 Hz, 4H), 1.05-1.09 (sextet, J= 7.45 Hz, 4H), 0.69-0.71 (t, J= 7.29 Hz, 6H). MALDI-TOF MS: $C_{26}H_{26}I_2N_2O_2$ calculated for: 652.31; found: 652.0172 (100%, [M + H]).

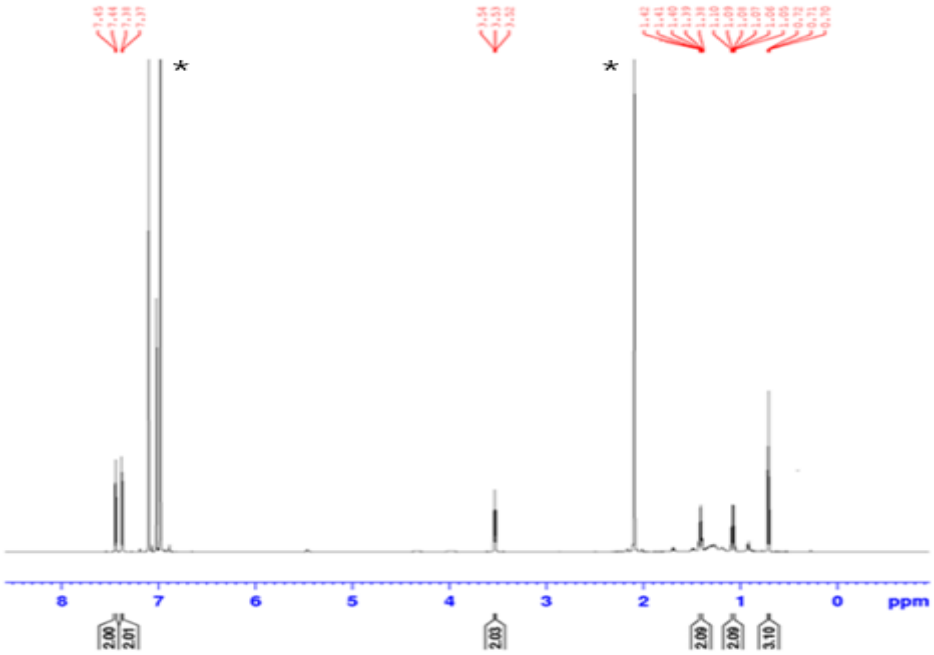

Fig. S3. ^{1}H NMR spectra of DPP-I 2.

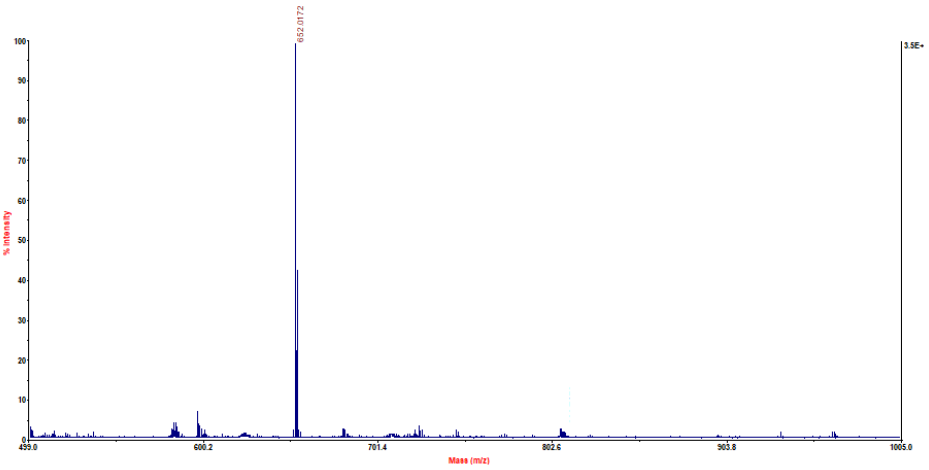

Fig. S4. MALDI-TOF mass spectra of DPP-I 2.

S1.2.3. DPP-COOH [1]

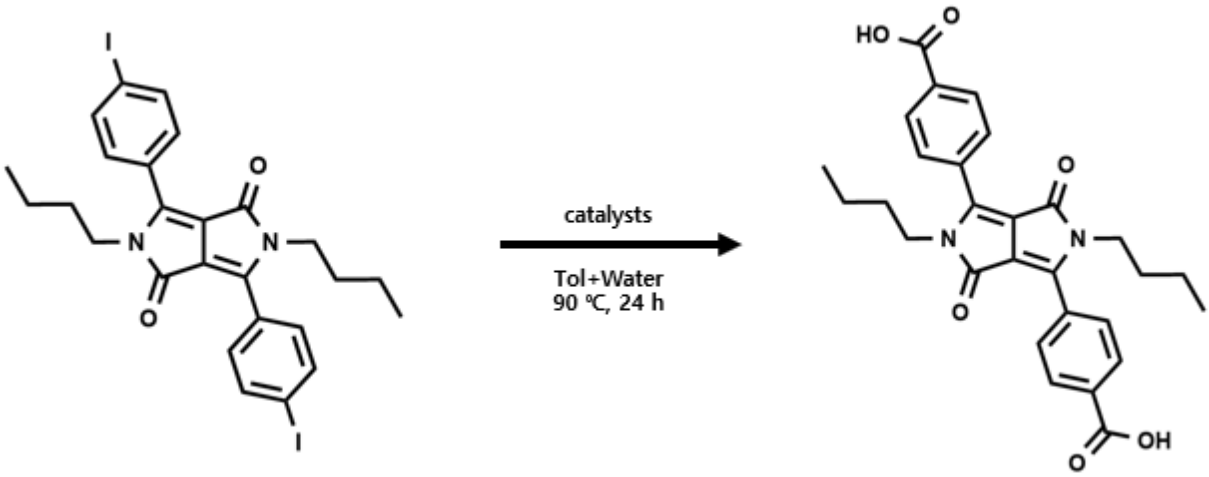

Scheme S4. Synthesis of DPP-COOH.

DPP I 2 (0.057 g, 0.081 mmol), Pd acetate (0.00256 g, 0.0114 mmol), XantPhos (0.0132 g, 0.0228

mmol), dimethylaminopyridine (0.012 g, 0.081 mmol), cobalt carbonyl (0.011 g, 0.032 mmol), and a mixture of toluene (7 ml) and water (3 ml) were mixed and sealed immediately, then stirred for 20 h at 90 ℃. After the reaction was completed, the mixture was cooled to room temperature. The reaction mixture was then poured into an aqueous citric acid solution (10 wt%) and extracted with ethyl acetate. The combined organic layers were dried over anhydrous $MgSO_4$ and dried in vacuum. The crude product was purified using a mixed solution by column chromatography on silica gel (MC: MeOH=30:1).

Yield: 36%; ^{1}H NMR (850 MHz, N,N-Dimethylformamide-*d7*): δ= 11.36 (s, 2H), 7.32 (d, J=8.50 Hz, 4H), 6.65-6.66 (d, J=8.50 Hz, 4H), 3.52-3.54 (t, J= 7.30 Hz, 4H), 1.60-1.63 (quintet, J= 2.80 Hz, 4H), 1.28-1.22 (sextet, J= 7.65 Hz, 4H), 0.87-0.89 (t, J= 7.40 Hz, 6H). MALDI-TOF MS: $C_{28}H_{28}N_2O_6$ calculated for: 488.54; found: 489. 1602 (100%, [M + H]).

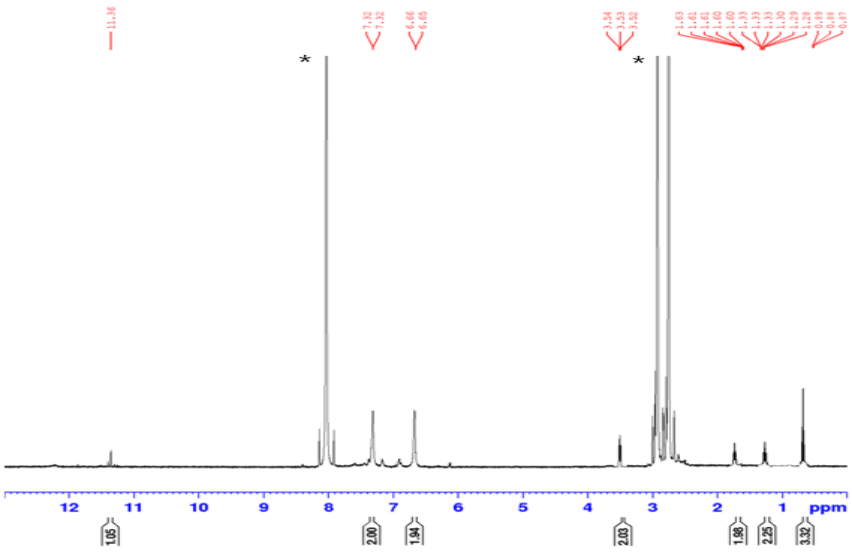

Fig. S5. ^{1}H NMR spectra of DPP-COOH.

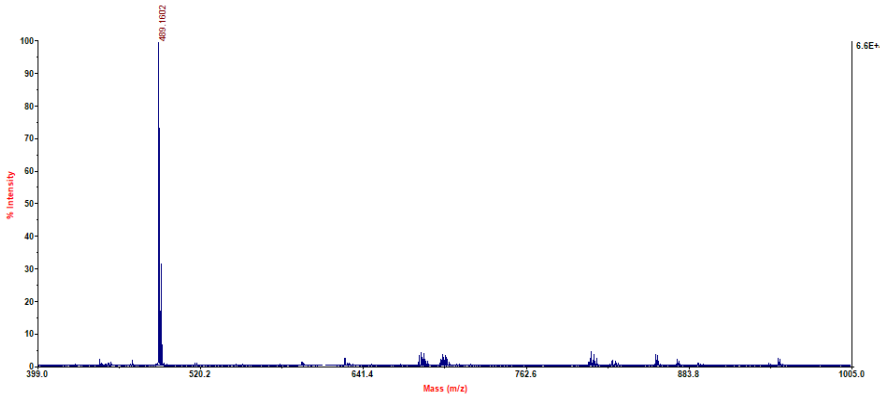

Fig. S6. MALDI-TOF mass spectra of DPP-COOH.

S1.3. Azo 1 [2]

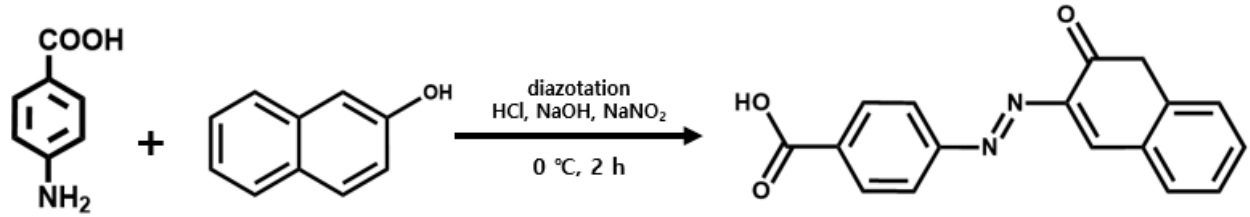

Scheme S5. Synthesis of Azo 1.

4-aminobenzoicacid (5 g, 36.45 mmol) was dissolved in a mixed solution of concentrated HCl (12 ml) and water (40 ml) and stirred in an ice bath held temperature of 0 ℃. A cooled mixture of sodium

nitrite (2.51 g) and water (20 ml) was added dropwise and stirred at that temperature. A coupling agent was prepared by dissolving 2-naphthol (5.256 g, 36.45 mmol) into an aqueous NaOH solution (5 g, in 50 ml water). The previously prepared diazonium salt was added dropwise to the coupling agent and stirred for 1 h at 0 ℃. The product was filtered and dried in vacuum and precipitated by a mixed solution of acetic acid and water to yield an Azo 1 dye.

Yield: 70.7%; ^{1}H NMR (500 MHz, CD_2Cl_2): δ=12.70 (s, 1H), 8.70 (s, 1H), 8.06-8.07 (d, J= 8.0 Hz, 2H), 7.60-7.61 (d, J= 8.4 Hz, 2H), 7.35-7.36 (t, J= 8.8 Hz, 1H), 7.34 (d, J= 7.6 Hz, 1H), 7.33 (d, J= 7.6 Hz, 1H), 7.22-7.23 (t, J= 7.4 Hz, 1H), 4.24 (s, 2H). MALDI-TOF MS: $C_{17}H_{12}N_2O_3$ calculated for: 292.29; found: 293.0324 (100%, [M + H]).

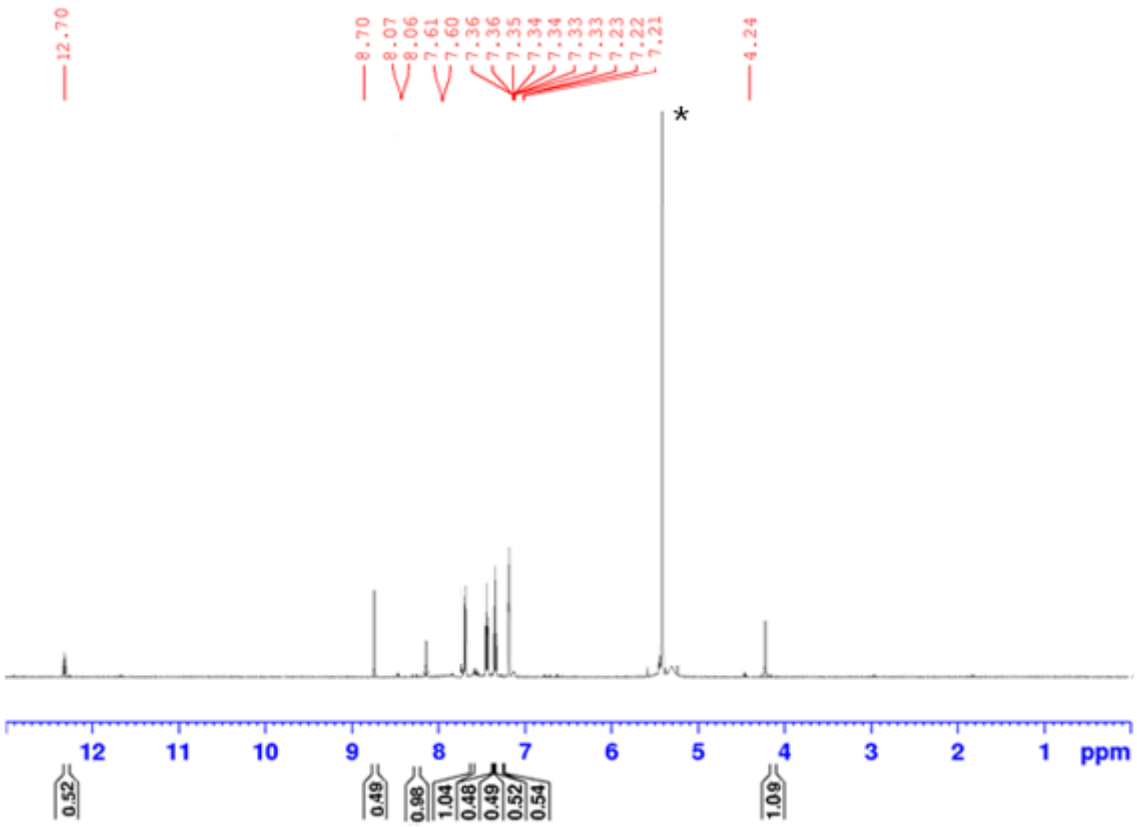

Fig. S7. ^{1}H NMR spectra of Azo 1.

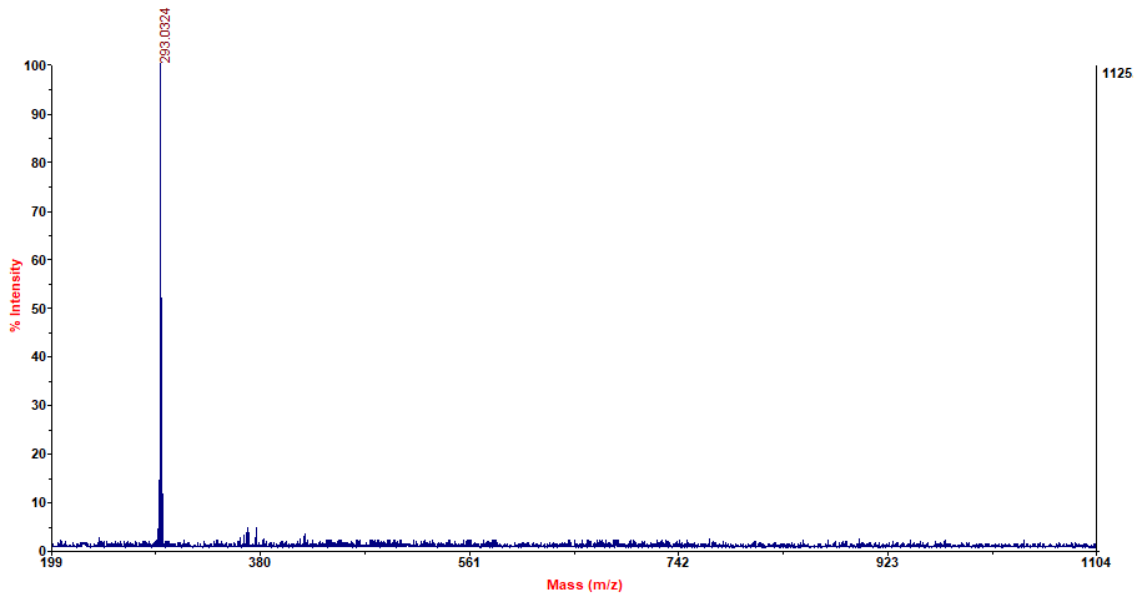

Fig. S8. MALDI-TOF mass spectra of Azo 1.

S1.4. Synthesis of TiO_2.

S1.4.1. PHT (precipitation + hydrothermal treatment) TiO_2 nanoparticle synthesis

Anatase TiO_2 powder was synthesized using hydrolysis, precipitation, and hydrothermal methods. Hydrolysis proceeded by slowly dripping titanium (IV) chloride (5 mL) into a sulfuric acid solution (H_2SO_4 10 mL: deionized water 50 mL) in an ice bath. Ammonium hydroxide solution (70 mL) was added to the precursor solution at 80 ℃. After 30 min of stirring and cooling to room temperature, the precipitate was washed three times through a centrifuge. The hydrothermal process was performed at 100 ℃ for 12 h using a Teflon-lined autoclave. After the reaction, the synthesized powder was filtered through a centrifuge and dried overnight in a vacuum oven at 70 ℃. The X-ray diffraction (XRD) was used to confirm the anatase phase, and the spherical morphology and uniform distribution of titanium and oxygen were qualitatively obtained using field emission SEM (FE-SEM) and energy dispersive spectroscopy (EDS) composition analysis. A specific surface area value of 118.7914 m^2/g was obtained using BET analysis.

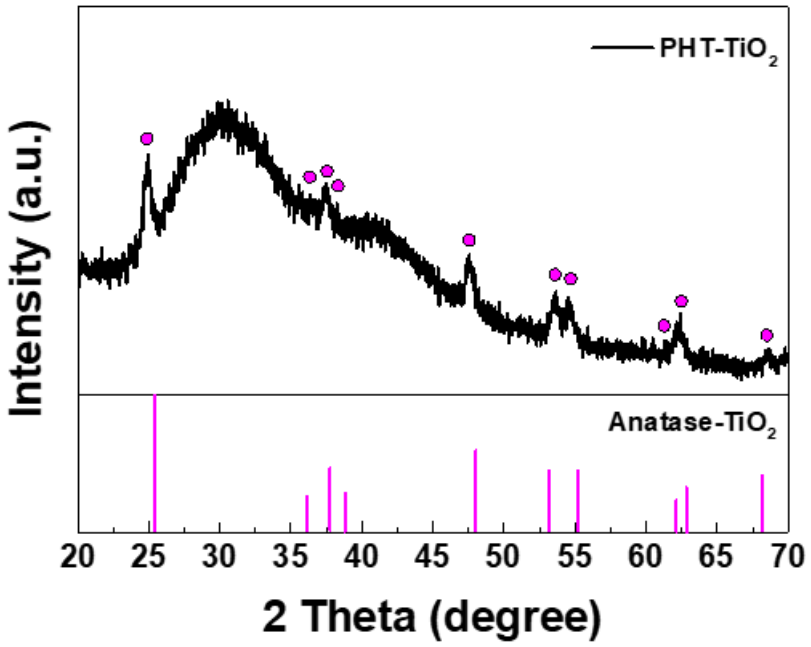

Fig. S9. XRD spectra of PHT-TiO_2 nanoparticles

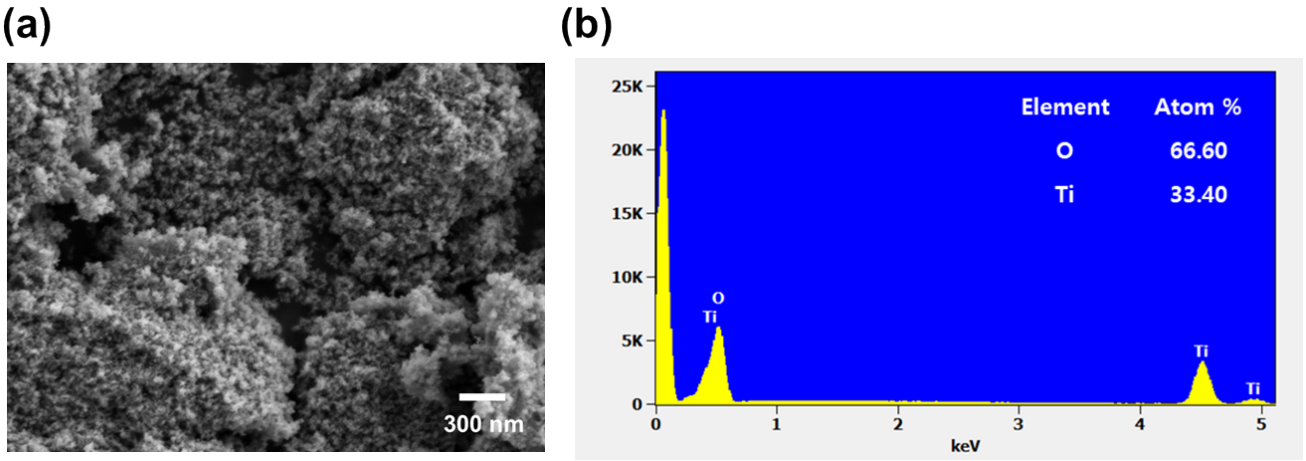

Fig. S10. (a)FE-SEM images and (b) EDS spectra of PHT-TiO_2 nanoparticles

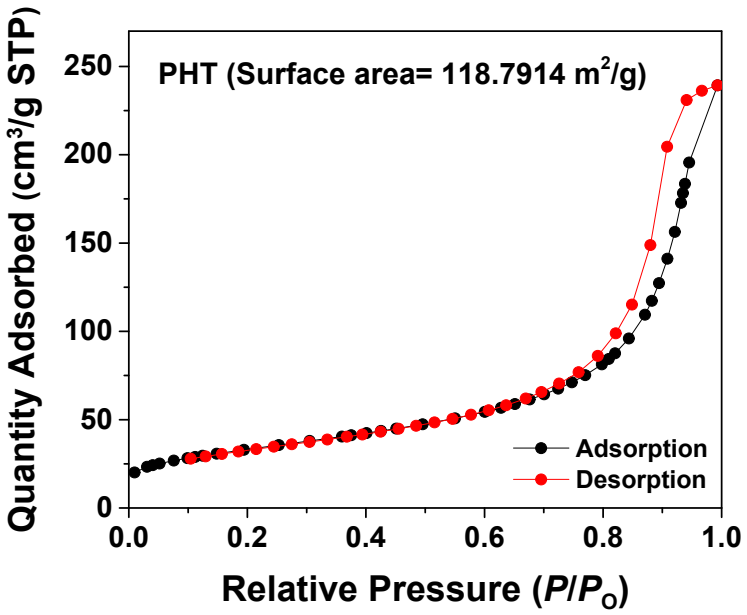

Fig. S11. N_2 adsorption-desorption isotherms and BET surface areas of PHT-TiO_2 nanoparticles

S1.4.2. HT (hydrothermal treatment) TiO_2 nanoparticle synthesis

Rutile TiO_2 powder was synthesized using hydrolysis and hydrothermal methods. Hydrolysis proceeded by slowly dripping titanium (IV) chloride (5 mL) into a sulfuric acid solution (H_2SO_4 10 mL: deionized water 50 mL) in an ice bath. The hydrothermal process was performed in a Teflon-lined autoclave for 12 h at 100℃. After the reaction, the synthesized powder was filtered through a centrifuge and dried overnight in a vacuum oven at 70 ℃. XRD analysis was used to confirm the rutile phase, and the needle-like morphology and uniform distribution of titanium and oxygen were qualitatively obtained using FE-SEM and EDS composition analysis. A specific surface area value of 45.2712 m^2/g was obtained using BET analysis.

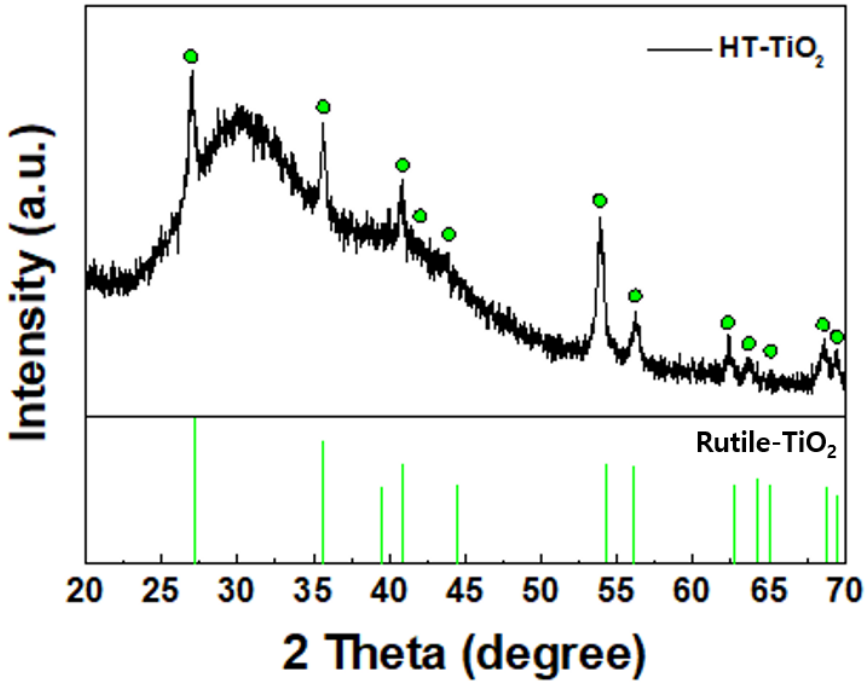

Fig. S12. XRD spectra of HT-TiO_2 nanoparticles

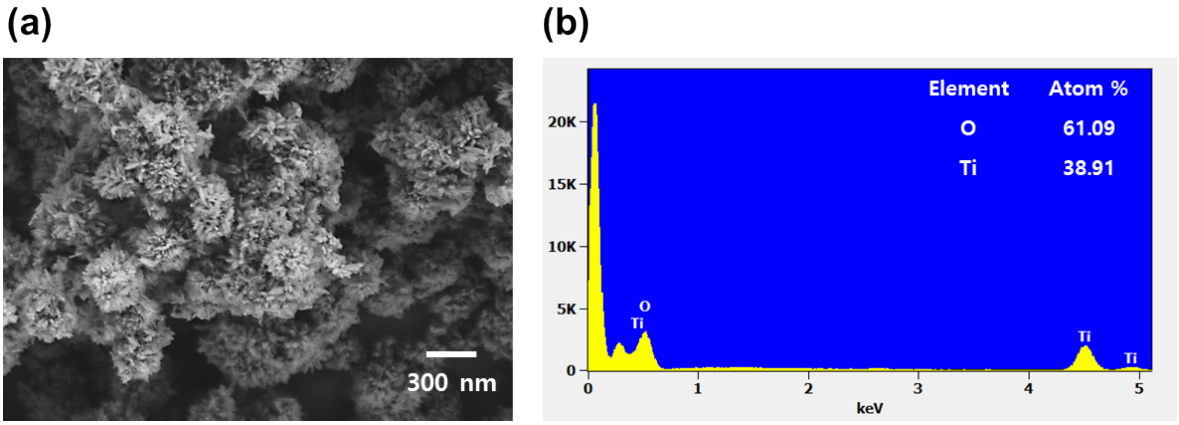

Fig. S13. (a)FE-SEM images and (b) EDS spectra of HT-TiO_2 nanoparticles

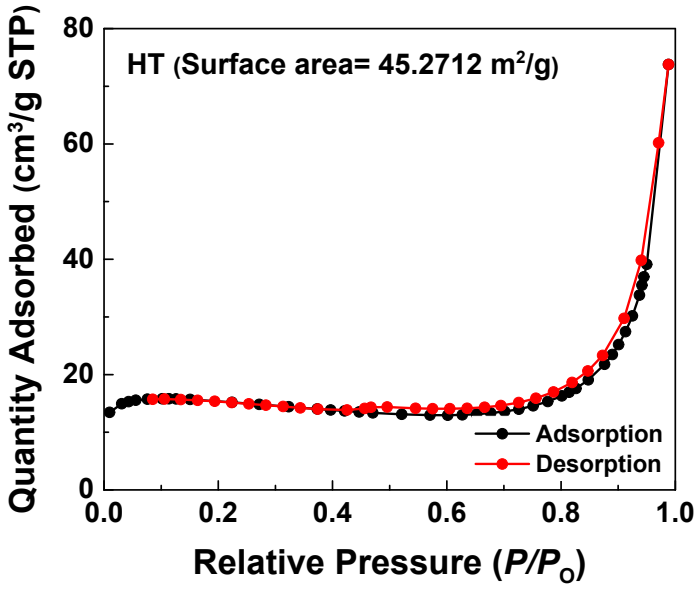

Fig. S14. N_2 adsorption-desorption isotherms and BET surface areas of HT-TiO_2 nanoparticles

S1.5. Average particle size of TiO_2 nanoparticles

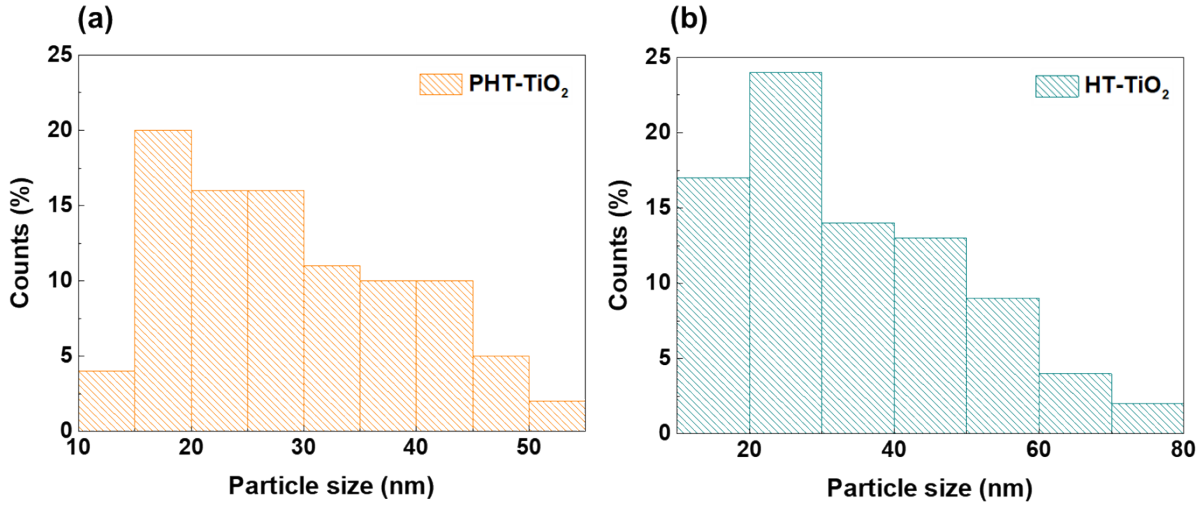

Fig. S15. Particle size distribution of (a) PHT, (b) HT TiO_2 nanoparticles

The average particle size of the nanoparticles was measured using the FE-SEM and ImageJ programs, and the sizes of 25.536 nm in the PHT-TiO_2 nanoparticles and 34.086 nm in the HT-TiO_2 nanoparticles in the HT sample were confirmed. PHT-TiO_2 nanoparticles with smaller average

particle sizes and larger specific surface areas than PH-TiO_2 nanoparticles were selected.

S1.6. FT-IR investigation.

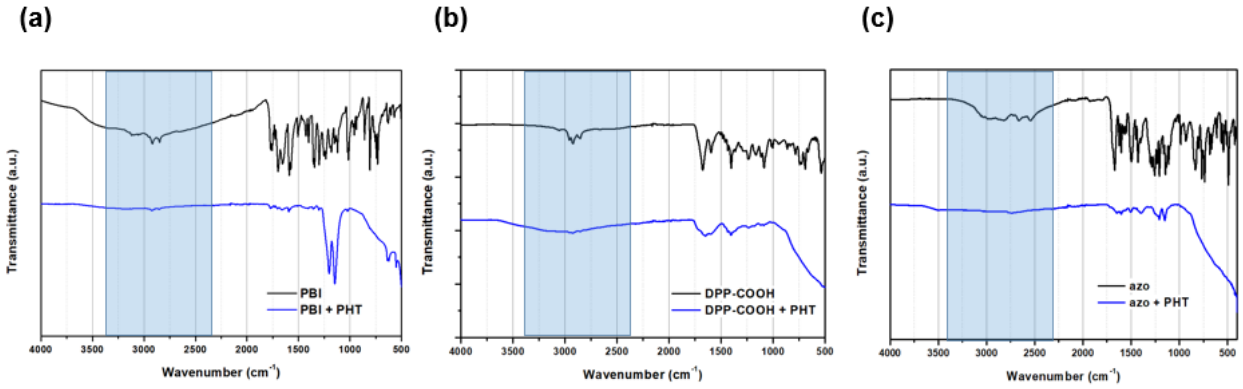

Fig. S16. Fourier transform infrared spectroscopy (FT-IR) spectra of the hybrid materials (a) PBI 2, (b) DPP-COOH, (c) Azo 1.

Around 2400-3400 cm^{-1}, the O-H stretch characteristic of carboxylic acid became weaker in the adsorbed samples, indicating the chemisorption of dye onto TiO_2. Furthermore, there were alterations in peak positions and intensities, along with the emergence of new peaks. Peaks below 1500 cm^{-1} changed, which can be associated with the vibrational modes related to the dye-dye interaction. Also, peaks around 1500-2000 cm^{-1} change positions and intensities, indicating weak interactions between the dye and the TiO_2 surface, such as van der Waals forces. Also, around 1600 cm^{-1}, the intensity of the peaks became weaker, indicating the O-H bending vibration of hydrogen bonding between TiO_2 and dye [3]. These changes provide evidence of the adsorption of TiO_2 and the dye.

S1.7. SEM images of the hybrid materials.

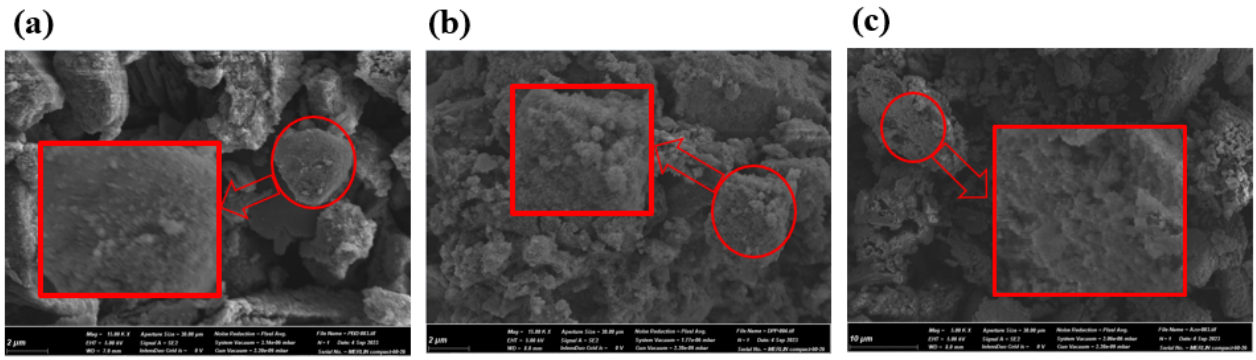

Fig. S17. SEM images of the hybrid materials (a) PBI 2, (b) DPP-COOH, (c) Azo 1.

Three samples were prepared in the solution state (0.5 mM of dye concentration, 4 mg of TiO_2 in 5 ml of MEK), stirred for one day for adsorption, and then dried in an oven at 85 ℃. Microscopic images of each hybrid material were obtained using SEM. Compared with the SEM image of TiO_2 (Fig. S10), hybrid materials exhibited more uneven particle size and rough surfaces, indicating dye and TiO_2 adsorption (Fig. S17).

S1.8. Relative absorbance during photodegradation

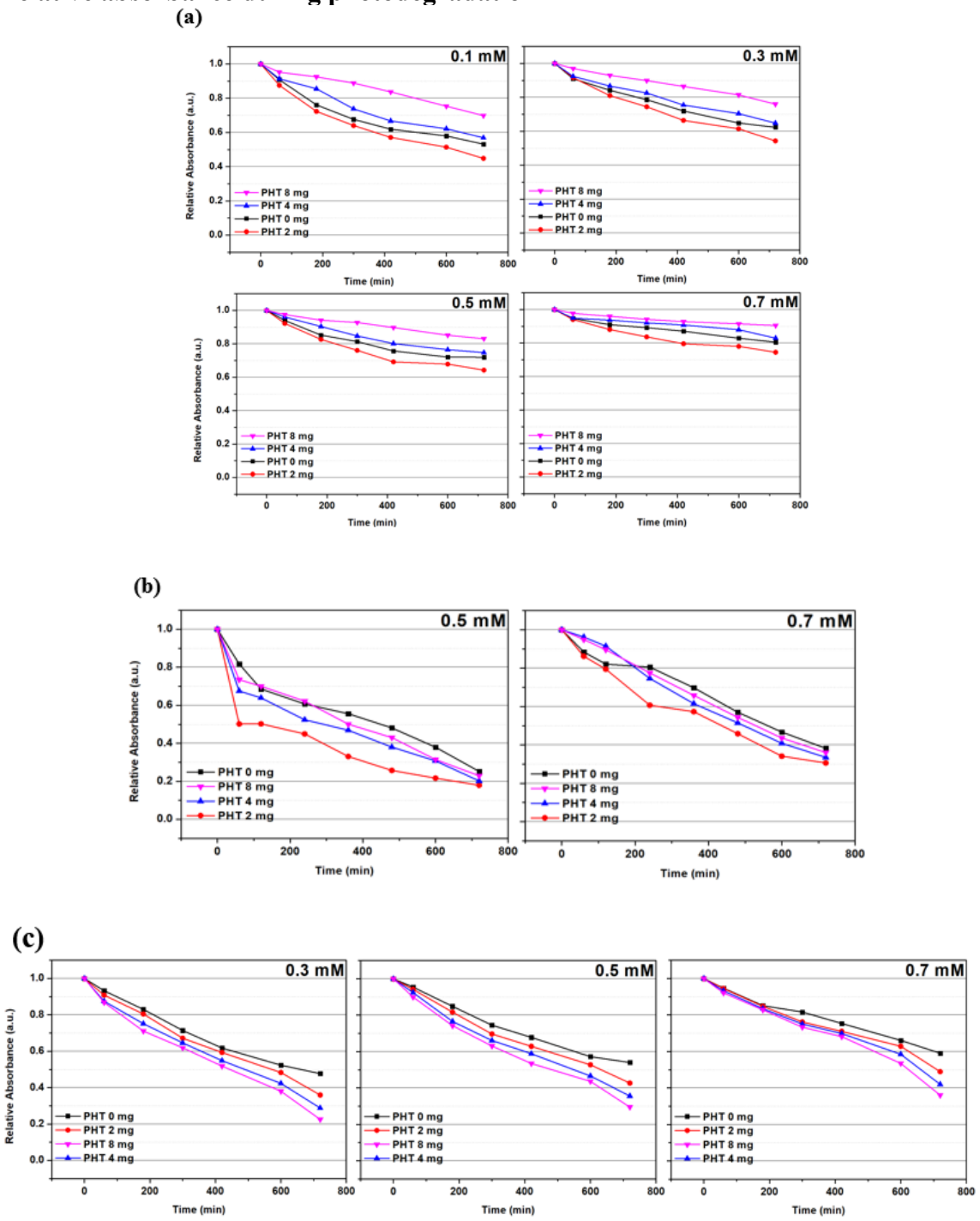

Fig. S18. Relative absorbance during photodegradation for 12 h (a) PBI 2, (b) DPP-COOH, (c) Azo 1.

* The absorbance at 0.1 and 0.3 mM for DPP-COOH and 0.1 mM for Azo 1 was insufficient to trust the photostability test result; therefore, excluded.

S1.9. L'a'b' values of the hybrid materials in films

Table S1. L'a'b' values and Δ E_{ab} of PBI 2 and PBI 2-hybrid material before and after thermal treatment. (a) 230 ℃-1 h, (b) 300 ℃-5 min

(a)		**L***	**A**	**B**	**Δ E_{ab}**
0 mg	Before	89.73	24.52	18.66	**10.85**
	After	85.66	27.73	28.19	
2 mg	Before	99.13	11.83	8.67	**8.58**
	After	90.98	9.81	6.96	
4 mg	Before	91.62	6.22	9.41	**8.44**
	After	99.43	9.32	8.62	
8 mg	Before	93.08	16.33	12.24	**2.92**
	After	95.54	17.03	10.85	

(b)		**L***	**A**	**B**	**Δ E_{ab}**
0 mg	Before	85.80	16.87	17.32	**8.71**
	After	91.81	19.61	23.00	
2 mg	Before	96.10	12.02	10.13	**5.18**
	After	98.02	9.46	6.05	
4 mg	Before	85.91	4.62	10.54	**2.94**
	After	88.65	5.67	10.68	
8 mg	Before	95.14	12.37	11.59	**1.29**
	After	95.68	13.55	11.63	

Table S2. L'a'b' values and Δ E_{ab} of DPP-COOH and DPP-COOH-hybrid material before and after thermal treatment. (a) 230 ℃-1 h, (b) 300 ℃-5 min

(a)		**L***	**A**	**B**	**Δ E_{ab}**
0 mg	Before	91.26	9.83	35.45	**61.63**
	After	39.10	0.13	4.10	
2 mg	Before	90.36	15.90	39.18	**59.13**
	After	44.10	0.29	5.51	
4 mg	Before	90.26	0.28	5.59	**50.59**
	After	39.47	0.56	3.68	
8 mg	Before	78.16	1.35	22.13	**46.09**
	After	33.02	1.14	12.80	

(b)		**L***	**A**	**B**	**Δ E_{ab}**
0 mg	Before	90.12	9.70	32.55	**54.41**
	After	37.36	5.54	19.94	
2 mg	Before	86.46	16.39	42.53	**53.35**
	After	37.23	8.42	23.57	
4 mg	Before	85.63	0.78	17.16	**50.59**
	After	42.67	0.27	4.04	
8 mg	Before	86.46	0.44	5.04	**46.09**
	After	44.72	0.19	2.81	

Table S3. L'a'b' values and Δ E_{ab} of Azo 1 and Azo 1-hybrid material before and after thermal treatment. (a) 230 ℃-1 h, (b) 300 ℃-5 min

(a)		**L***	**A**	**B**	**Δ E_{ab}**
0 mg	Before	79.77	15.17	38.64	**18.50**
	After	92.22	4.92	29.58	
2 mg	Before	77.65	8.75	30.87	**15.53**
	After	86.32	11.20	43.52	
4 mg	Before	92.89	6.64	21.71	**11.45**
	After	99.03	2.38	13.03	
8 mg	Before	79.71	11.31	34.76	**4.96**
	After	82.97	7.57	34.61	

(b)		**L***	**A**	**B**	**Δ E_{ab}**
0 mg	Before	86.27	11.72	32.36	**12.62**
	After	83.48	12.40	44.65	
2 mg	Before	73.07	14.93	39.85	**7.95**
	After	79.66	13.61	44.11	
4 mg	Before	95.06	6.99	22.57	**5.45**
	After	89.64	6.45	22.43	
8 mg	Before	95.83	6.27	19.13	**1.73**
	After	96.15	4.60	19.48	

S1.10. ESR signal intensity of the hybrid materials

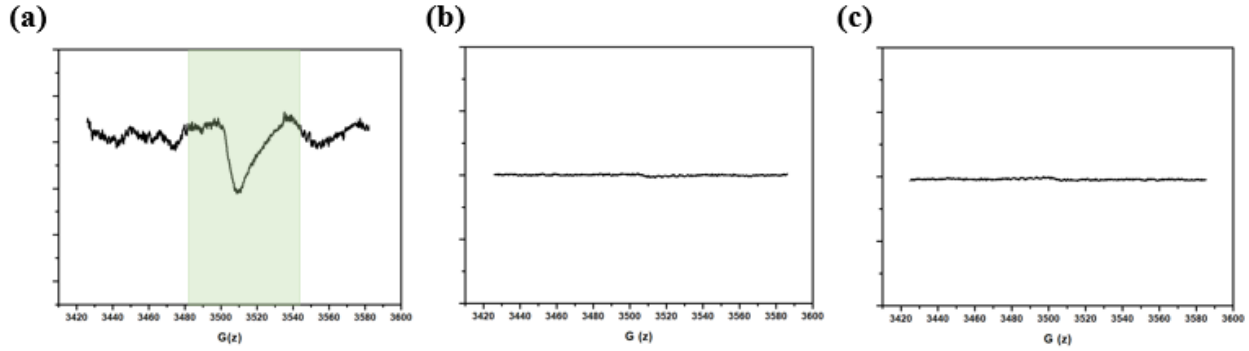

Fig. S19. ESR signal intensity of PBI 2-hybrid material according to TiO_2 concentration.

(a) 2 mg, (b) 4 mg, (c) 8 mg.

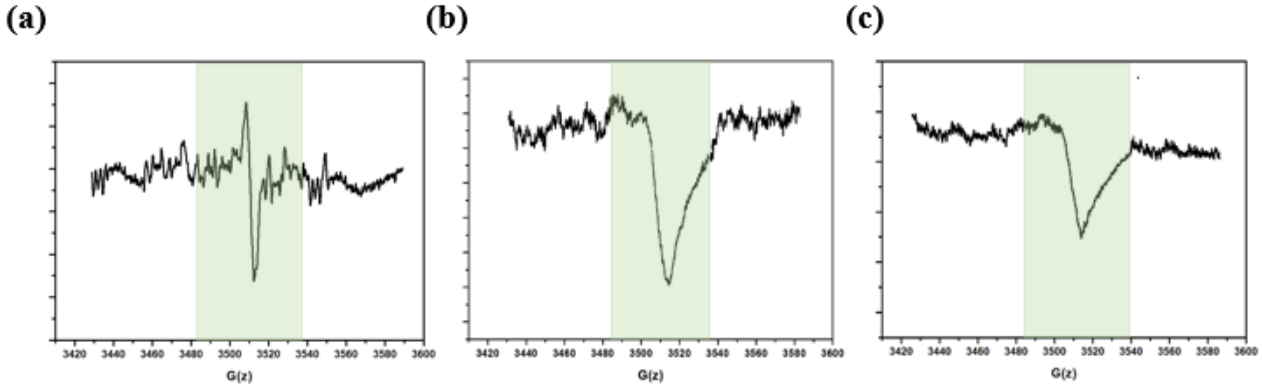

Fig. S20. ESR signal intensity of DPP-COOH-hybrid material according to TiO_2 concentration.

(a) 2 mg, (b) 4 mg, (c) 8 mg.

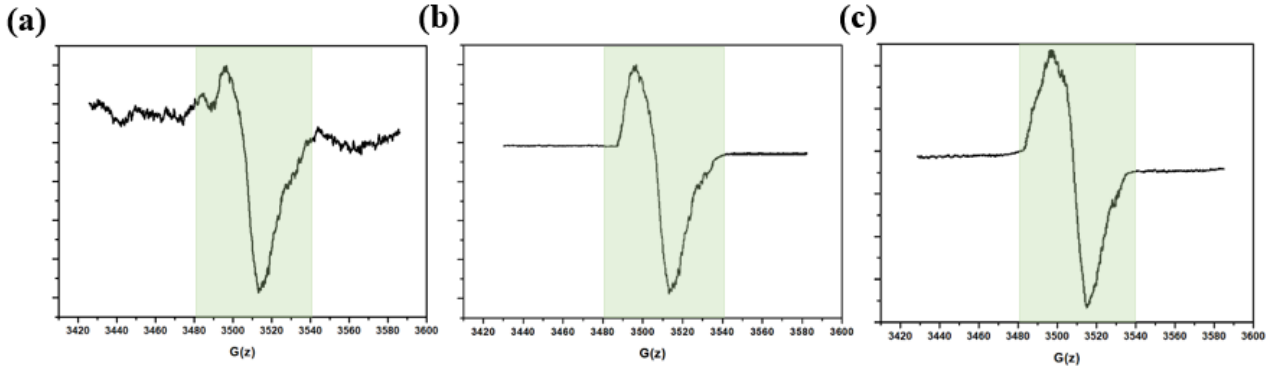

Fig. S21. ESR signal intensity of Azo1-hybrid material according to TiO_2 concentration.

(a) 2 mg, (b) 4 mg, (c) 8 mg.

S1.11. Solvent investigation

The toxicity, boiling point, solubility, compatibility with the manufacturing process, and impact on the adsorption amount are factors to consider when selecting a suitable solvent for adsorbing TiO_2 and the dyes involved [4-6]. MEK emerged as a promising choice because of its low toxicity, boiling point of approximately 80 ℃, and established color filter use [7]. Aprotic solvents, such as MEK, offer distinct advantages over protic solvents for the adsorption of TiO2 and dyes [5]. Furthermore, all three dyes exhibited some solubility in MEK (Table S4). Considering these factors, the hybrid materials were prepared by adsorbing TiO2 and dyes using MEK as the solvent.

Table S4. Solubilities of the dyes in MEK solution.

	Toluene	MC	Acetone	DMF	MEK	NMP	DMSO	Ethanol	Methanol
PBI 2	--	--	-	+	+	+	+	+	+
DPP-COOH	+	+	++	++	++	++	++	++	++
Azo 1	+	++	++	++	++	++	++	++	++

* grade was indicated from -- (very low solubility) to ++ (excellent solubility)

S1.12. Experimental investigation of intramolecular charge transfer

Table S5. Maximum absorption wavelengths of dyes in solvents in order of increasing polarity**.**

	1,4-dioxane	Toluene	MC	Acetone	MeOH	DMF
PBI 2	524.5	526	525	522.5	523	526
DPP-COOH	487.5	488	486.5	486	485	485
Azo 1	479.5	482	484.5	486	488.5	491

Only Azo 1 showed a bathochromic shift in the maximum absorption wavelength as the polarity of the solvent increased, indicating that ICT occurred.

References

1. M. J. Ritesh Haldar, Antoine Mazel, Qiang Zhang, Alexander Welle, Tawheed Mohamed, Peter Krolla, Wolfgang Wenzel, Stéphane Diring, Fabrice Odobel, Bryce S. Richards, Ian A. Howard & Christof Wöll, Anisotropic energy transfer in crystalline chromophore assemblies, *nature communication*, 2018, **9, 4332 (2018)**.
2. N. T. LUKA MATOVIC, NEMANJA TRISOVIC, JELENA LADAREVIC, VESNA VITNIK, On the az On the azo dyes deriv es derived from benz om benzoic and cinnamic acids used as oic and cinnamic acids used as photosensitizers in dye-sensitized solar cells *Turkish Journal of Chemistry*, 2019, **43, 4 (2019)**.
3. F. W. l. Barbara Völker, Thomas Bürgi, and Dominic Lingenfelser, Dye Bonding to TiO2: In Situ Attenuated Total Reflection Infrared Spectroscopy Study, Simulations, and Correlation with DyeSensitized Solar Cell Characteristics, *Langmuir*, 2012, **2012, 28, 11354–11363**.
4. M. A. Hironobu Ozawa, Takahiko Ono, and Hironori Arakawa, Effects of Dye-Adsorption Solvent on the Performances of the Dye-Sensitized Solar Cells Based on Black Dye, *Chemistry – An Asian Journal*, 2012, **2012, 7, 156-162**
5. J. M. Hui Fang, Michael J. Wilhelm, Brendan G. DeLacy, Hai-Lung Dai, Influence of Solvent on Dye-Sensitized Solar Cell Efficiency: What is so Special About Acetonitrile?, *Particle&particle sysyems characterization*, 2021, **2021, 38, 2000220**.
6. T. Y. Takahiko Ono, Hironori Arakawa, Influence of Dye Adsorption Solvent on the Performance of a Mesoporous TiO2 Dye-Sensitized Solar Cell Using Infrared Organic Dye *Journal of Solar Energy Engineering*, 2010, **132(2): 021101**.
7. S.-W. C. Kea-Tiong Tang, Meng-Fan Chang, Chih-Cheng Hsieh, Jyuo-Min Shyu, A Low-Power Electronic Nose Signal-Processing Chip for a Portable Artificial Olfaction System, *IEEE Transactions on Biomedical Circuits and Systems*, 2011, **5 issue: 4**.